Applied Surface Science 311 (2014) 643–647

Contents lists available at ScienceDirect

Applied Surface Science

journal homepage: www.elsevier.com/locate/apsusc

11-Hydroxyundecyl octadecyl disulfide self-assembled monolayers on Au(1 1 1)

Erol Albayrak[a], Semistan Karabuga[b], Gianangelo Bracco[c], M. Fatih Danışman[d,*]

[a] Department of Materials and Metallurgical Engineering, Ahi Evran University, Kırşehir 40000, Turkey
[b] Department of Chemistry, Kahramanmaraş Sütçü İmam University, Kahramanmaraş 46030, Turkey
[c] CNR-IMEM and Department of Physics, University of Genoa, via Dodecaneso 33, Genoa 16146, Italy
[d] Department of Chemistry, Middle East Technical University, Ankara 06800, Turkey

ARTICLE INFO

Article history:
Received 2 May 2014
Received in revised form 15 May 2014
Accepted 16 May 2014
Available online 28 May 2014

Keywords:
Unsymmetric disulfides
Self-assembled monolayers
Au(1 1 1)
Helium diffraction
Low energy atom scattering
Supersonic molecular beam deposition

ABSTRACT

Here, we report a helium atom diffraction study of 11-hydroxyundecyl octadecyl disulfide (CH_3—$(CH_2)_{17}$—S—S—$(CH_2)_{11}$—OH, HOD) self-assembled monolayers (SAMs) produced by supersonic molecular beam deposition (SMBD). Two different lying down monolayer phases were observed depending on the substrate temperature. At low temperatures a poorly ordered phase was observed, while the diffraction patterns of the film grown at high temperatures were similar to that of mercaptoundecanol (MUD) SAMs reported previously in the literature. The transition from the low temperature phase to the high temperature phase is due to S—S bond cleavage at the surface. Desorption from several different chemisorbed and physisorbed states were observed with energies in the same range as observed for MUD and octadecanelthiol (ODT) SAMs.

1. Introduction

Thiol self-assembled monolayers (SAMs) on Au(1 1 1) surfaces continue to attract attention due to their uses in many different applications and their role as a model system in fundamental surface science [1–4]. Their fundamental properties, like crystal structures, adsorption dynamics and mechanism are very important to understand to improve the performance of the applications that utilize these SAMs [1–5].

Alkanethiol SAMs on Au(1 1 1) are well studied systems and at low coverage they adopt lying down striped phases with $(p \times \sqrt{3})$ rectangular unit cells where p is the stripe periodicity, as depicted in Fig. 1, which depends on the alkyl chain length.[1,2,6] At full coverage, however, thiol molecules stand up and form the well-known $(\sqrt{3} \times \sqrt{3})R30^\circ$ structure [1,2]. Unsymmetric disulfide (R—S—S—R′, will be referred to UDS) SAMs, on the other hand, are particularly important for preparing mixed monolayers and for understanding thiol film formation mechanism and kinetics. To this end, disulfides where the unsymmetry was provided by using alkyl groups with different chain lengths or with different functionalities (like hydroxylated and fluorinated ones) were intensively studied [7–16]. One of the main motivations in these studies was to elucidate whether a phase separation takes place or not, which has implications in preparation of patterned surfaces and which is a way of determining if S—S bond cleaves during adsorption. In all of these studies disulfides was grown from solution and the film coverage was controlled by adjusting the concentration of the solution and/or the immersion time. Resulting films were mostly studied by scanning probe microscopy and spectroscopy techniques. While in many cases no phase separation was observed for the as grown full coverage (high density) UDS SAMs [11–13], phase separation after annealing have also been reported [14,15]. In addition for 11-hydroxyundecyl octadecyl disulfide (CH_3—$(CH_2)_{17}$—S—S—$(CH_2)_{11}$—OH, HOD) SAM phase separation was reported at low coverage evidenced by the formation of two different corrugation periodicities consistent with the lengths of separated thiolates [10].

Here we present a helium atom diffraction study of the HOD SAMs grown in vacuum by means of supersonic molecular beam deposition (SMBD) which allows a very precise control of film coverage. Using helium diffraction enabled us to monitor film growth in real time and follow the evolution of film structure as a function coverage and substrate temperature. We identified two different lying down monolayer phases one of which was observed only when the film was grown at low substrate temperatures ($T \approx 200$ K).

* Corresponding author. Tel.: +90 0312 2107618; fax: +90 0312 2103200.
E-mail address: danisman@metu.edu.tr (M.F. Danışman).

http://dx.doi.org/10.1016/j.apsusc.2014.05.128
0169-4332/

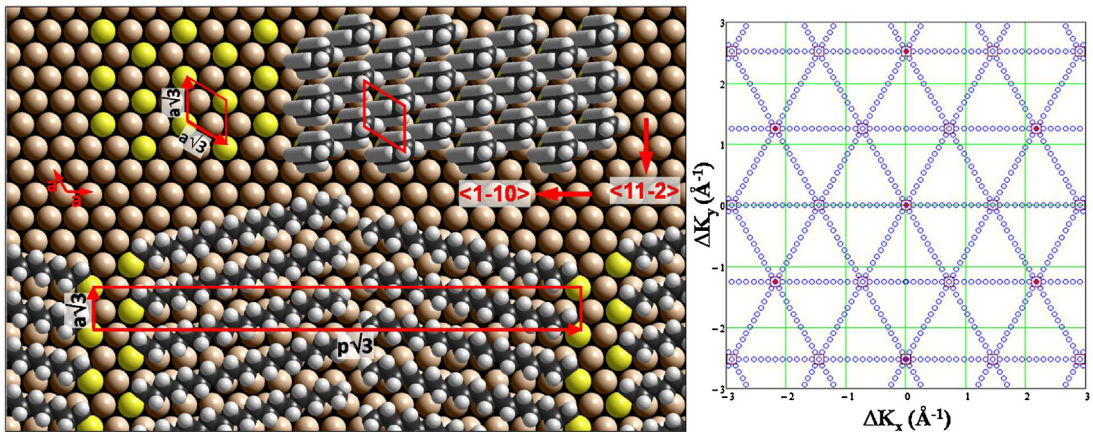

Fig. 1. Left panel: real space model of $(\sqrt{3} \times \sqrt{3})$R30° and $(p \times \sqrt{3})$ unit cell structure of octadecanethiol SAMs on Au(1 1 1). For octadecanethiol striped phase $p = 18$. (Sulfur atoms, indicated by yellow color, are placed on top of gold atoms for simplicity and this position does not correspond to the actual adsorption site.) Right panel: corresponding reciprocal space map. Red dots indicate gold diffraction peak positions, blue circles indicate $(p \times \sqrt{3})$ diffraction peak positions and the brown squares indicate $(\sqrt{3} \times \sqrt{3})$R30° diffraction peak positions. (For interpretation of the references to color in this figure legend, the reader is referred to the web version of this article.)

This low temperature (LT) phase irreversibly transformed into a different phase after annealing to 300 K. This high temperature (HT) phase could also be formed directly by depositing the HOD SAM at 300 K or higher substrate temperature. While both phases had poor helium diffraction patterns, upon annealing to 400 K, diffraction patterns of the HT phase improved considerably. A comparison of the diffraction results with that of pure mercaptoundecanol (MUD) and octadecanethiol (ODT) SAMs that we studied in the past [17] enabled us to comment on the crystal structure of the HOD SAMs. Finally we were able to determine desorption energies for several different chemisorbed states which were in the same range observed for pure MUD and ODT SAMs.

2. Experimental

The experimental setup was extensively described before [18,19] and here we give only a brief description related to the present experiment. The SMBD source is made of a Pyrex tube with a ≈100 μm diameter nozzle which is housed in a vacuum chamber connected to the main chamber of the diffraction apparatus. Inside the tube, a small Pyrex reservoir contains the organic material, outside the tube a coil heater increases the source temperature causing the sublimation of the organic material and its vapor mixes with the helium carrier. This mixture expands through the nozzle and forms a seeded beam. In front of the nozzle, a skimmer selects the central part of the flow which enters the main chamber of the diffraction apparatus where at its center is located the surface of the substrate. The SMBD temperature determines the partial pressure of the organic vapor and, for source temperatures in the range 160–180 °C, reasonable HOD flux values were obtained. Although the impinging energy of the HOD molecules were not directly measured, for a thiol concentration of less than 1% and assuming ideal expansion conditions to calculate the terminal speed of the carrier gas, the maximum incident kinetic energy has been estimated to be in the range 5.2–11.9 eV [20].

The diffraction experiments on the deposited films were carried out by using the primary supersonic beam of helium (purity 99.9999%). The source temperature was set to about 70 K which corresponds to a kinetic energy of 14 meV and hence the most probably wave vector was $k_i = 5.13$ Å^{-1} with a velocity spread of 2%. In order to reduce the effect of vibrations, diffraction intensities were collected for substrate temperatures between 60 K and 80 K along different crystallographic directions to reconstruct the unit cell of the structures. The detector is a Si bolometer, cooled to about 2 K with a pumped liquid helium cryostat, which can rotate around the sample in the plane containing the incident helium beam and the surface normal. For the analysis, the angular scale was converted to parallel momentum $\Delta K_{//}$scale by using the equation $\Delta K_{//} = k_i(\sin\theta_f - \sin\theta_i)$ where θ_i and θ_f are the incident angle and the detector angular position with respect to surface normal, respectively. The Au sample was purchased from Mateck GmbH with an orientation accuracy of <0.1° from the (1 1 1) surface. Before each experimental run, the surface was sputtered and annealed and to assess its cleanness the presence of the gold reconstruction in the diffraction pattern with specular reflection intensity of at least 25% of the incident beam was checked.

Desorption energies were investigated by recording helium specular reflection (SR) intensity as a function of surface temperature. In fact, the SR intensity decreases with temperature due to Debye–Waller effect and, above 400 K, to the decrease of the sensitivity of our detector. Since the substrate surface is smoother and harder than the film one, when the film starts to desorb the SR intensity increases until the whole film is desorbed and the SR intensity starts to decrease again due to the Debye–Waller factor of the substrate. The derivative of the SR intensity, corrected for Debye–Waller effect and detector sensitivity, vs. the sample temperature yields a conventional temperature programmed desorption peak [21]. The estimation of adsorption energies of the desorbing species is obtained by a Redhead analysis [22] and a first-order desorption and a coverage independent desorption energy were assumed (assumptions generally used in literature for similar analysis). The experiment was performed with crystal temperature ramps of 0.8–1.3 K/s and the error bars on the temperature measured by a platinum thermometer were estimated to be ±5 K.

HOD was synthesized as follows by following the procedure proposed by Flores et al. [11]: Octadecanethiol (3.5 mmol) was added to the solution of diethylazadicarboxylate (DEAD) (3.5 mmol) in 20 ml of diethyl ether at room temperature. The reaction mixture was stirred for 3 days. After evaporation of solvent at reduced pressure, the crude mixture was dissolved in 20 ml of dichloromethane (DCM). The mixture of reaction was added mercapto undecanethiol (3.5 mmol) and refluxed for 2 days, monitored by TLC. The solvent was concentrated under vacuum and the crude product was purified by column chromatography on silica eluting with hexane and ethyl acetate (v/v, 3:1) to yield as a white solid. Yield: 38%; mp 71–73 °C; 1*H* NMR (400 MHz, CDCl3, ppm) δ 3.64 (t, $J = 6.6$ Hz, 2*H*), 2.68 (t, $J = 7.3$ Hz, 4*H*), 1.66 (td, $J = 14.9$, 7.3 Hz, 4*H*), 1.61–1.51 (m, 2*H*), 1.45–1.19 (bm, 44*H*), 0.88 (t, $J = 6.8$ Hz, 3*H*).

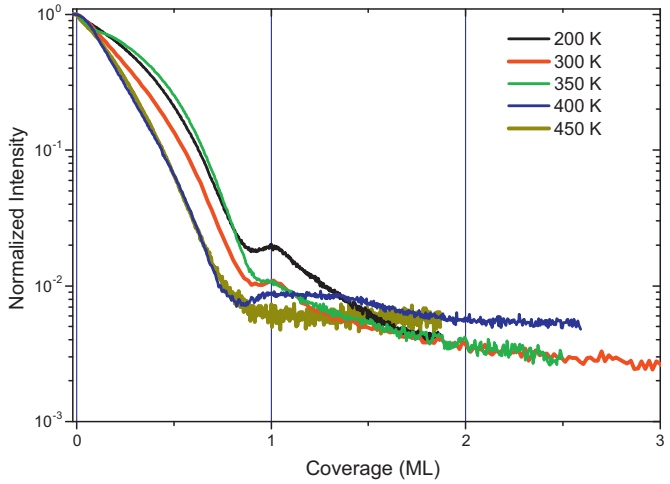

Fig. 2. Deposition curves showing helium specular reflection intensity as a function of HOD coverage on Au(1 1 1) at different substrate temperatures.

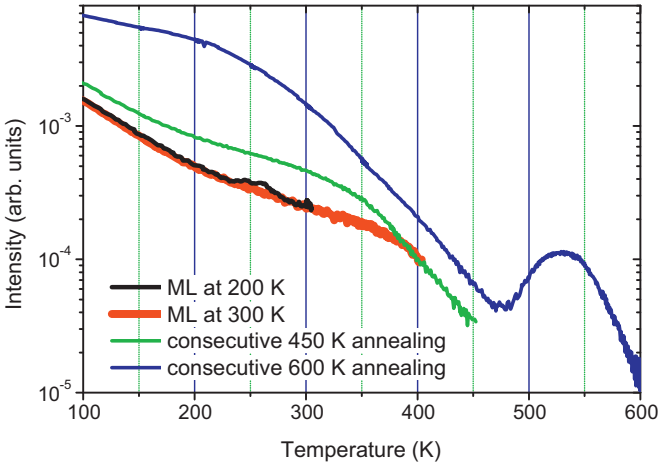

Fig. 4. Annealing curves that show the SR intensity as a function of surface temperature for different films indicated in the legend. The plots shown here are not corrected for the detector sensitivity and the Debye–Waller effect. (For interpretation of the references to color in this figure legend, the reader is referred to the web version of this article.)

3. Results

In Fig. 2 we show deposition curves where helium specular reflection (SR) intensity is plotted as a function of film coverage for different substrate temperatures. All the curves are normalized to the specular reflection intensity at zero coverage. A partial recovery of the SR with a maximum is observed for the majority of the curves and this is due to smoothening of Au(1 1 1)/HOD surface upon completion of the monolayer due to overlapping of the large effective helium cross sections of the adsorbed molecules yielding a more ordered film. Following the recovery, SR intensity decreases again with increasing coverage due to formation of disordered physisorbed overlayers. This trend is true for all the substrate temperatures studied except at 450 K for which no recovery could be observed due to a significant Debye Waller effect.

Diffraction scans from MLs grown at 200 K and 300 K, recorded at 80 K substrate temperature, are shown in Fig. 3. The diffraction pattern of the HOD film grown at 200 K (that will be referred to as low temperature, LT ML) presents very broad features and is completely different from that of the film grown at 300 K (that will be referred to as high temperature, HT ML). In fact, the HT ML diffraction pattern shows broad $\sqrt{3}$ peaks along the $\langle 1\,1\,-2\rangle$ direction and more defined diffraction peaks related to the striped phase along the $\langle 1\,-1\,0\rangle$ direction. When the LT ML is annealed to 300 K, the original diffraction pattern changes and assumes a structure similar to that of the HT ML (data not shown). To investigate the causes of formation of different ML structures, we studied the evolution of the film structure with substrate temperature by recording SR intensity as a function of substrate temperature (annealing curves shown in Fig. 4) and recording the resulting diffraction patterns (Fig. 5). When the annealing curve for the LT ML is examined (black trace in Fig. 4) a change in the slope can be observed to take place between 235 K and 290 K, which may be due to a phase transition, while a monotonic decay is observed for the HT ML in the same temperature range (red trace in Fig. 4). In the latter case no change is expected since the substrate temperature was already above 235–290 K range during deposition for the HT ML. This phase transition is most probably associated with the cleavage of S—S bonds and a readjustment of the molecular fragments: at 200 K, the HOD molecules adsorb intact resulting in the LT ML structure and during annealing to 300 K S—S bonds are dissociated into thiolates forming the HT ML phase. In fact, for dimethyl disulfide SAMs dissociation was shown to take place between 160 K [23] and 220 K [24].

When the 400 K annealing curve of the HT ML (red trace in Fig. 4) is further examined, at about 380 K an increase in the decay rate can be observed which is due to the starting of a solid–liquid

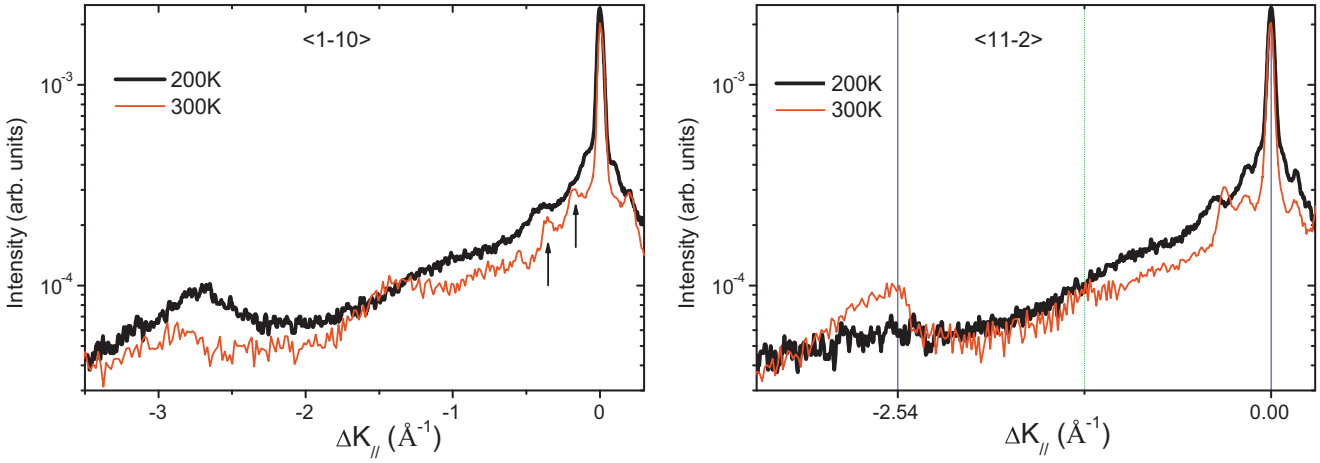

Fig. 3. Diffraction scans measured at 80 K along the main azimuthal directions of Au(1 1 1) for ML films of HOD grown at different substrate temperatures. The arrows in the left plot indicate striped phase peak positions and the vertical line at $\Delta K_{//} = -2.54\,\text{Å}^{-1}$ in the right plot indicates the $\sqrt{3}$ peak position.

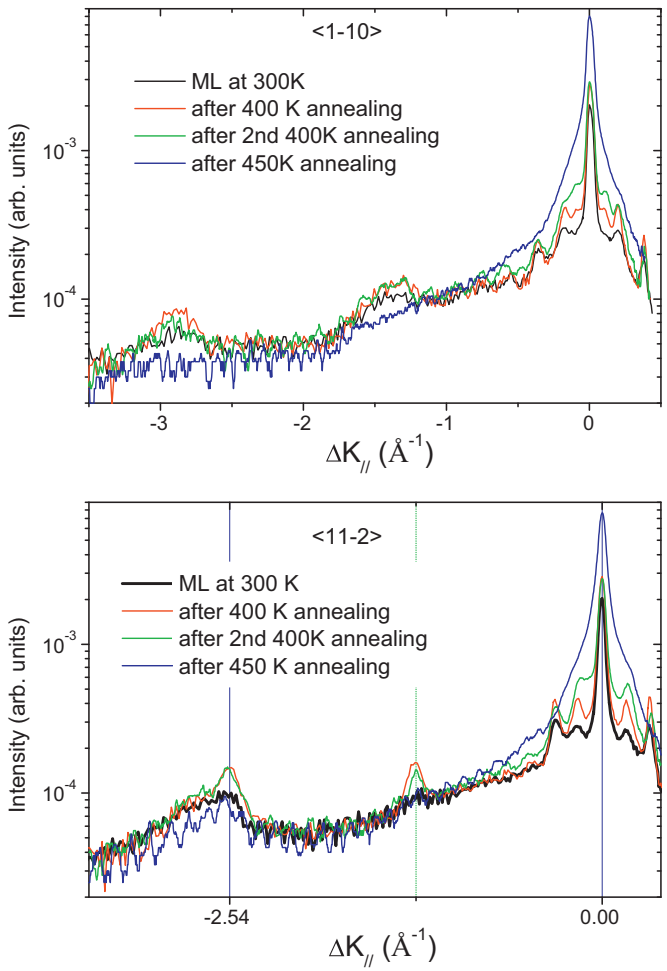

Fig. 5. Diffraction scans of ML film grown at 300 K substrate temperature after different thermal treatment steps. The oscillations in the blue curves, most pronounced at low intensities, are due to noise as discussed in the text. (For interpretation of the references to color in this figure legend, the reader is referred to the web version of this article.)

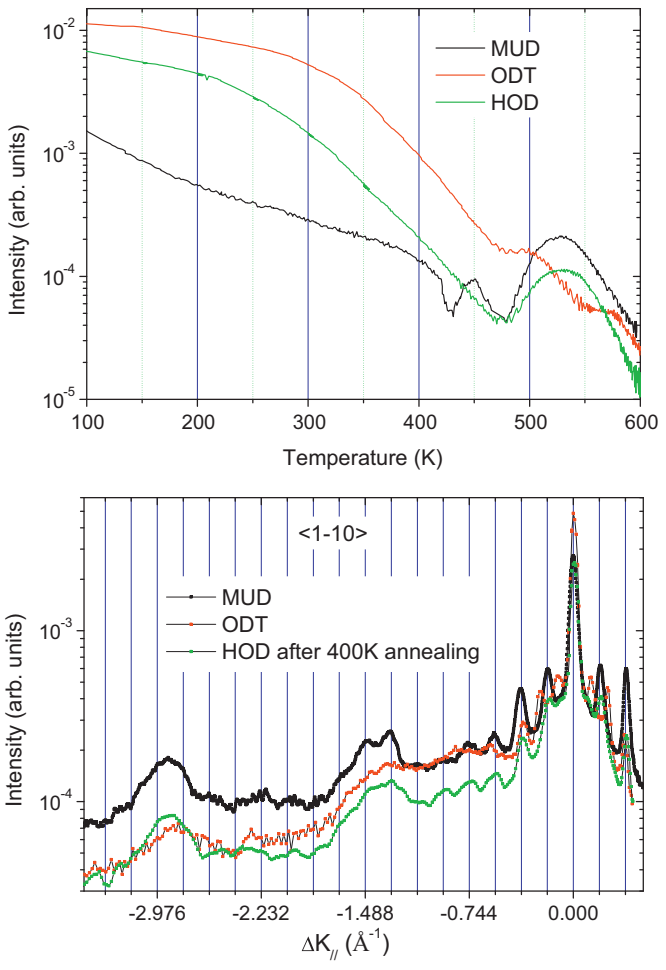

Fig. 6. (a) Annealing curves for MLs of MUD, ODT and HOD. (b) Diffraction scans of MLs of MUD, ODT and HOD. Grid lines indicated the expected peak positions for $(11.8 \times \sqrt{3})$ unit cell. HOD diffraction scan is smoothed by adjacent point averaging for clarity.

phase transition which was observed before for different thiol SAMs [6,17,25,26]. After 400 K annealing, the resulting film has an improved diffraction pattern with sharper and more intense peaks without a change in the peak positions (compare the black and red traces in Fig. 5). Further annealing at 400 K, however, does not improve the diffraction pattern. After annealing at 450 K, SR peak intensity increased considerably and all the diffraction peaks vanished except the very broad $\sqrt{3}$ peak along the $\langle 1\,1\,-2\rangle$ direction. This is a clear sign that the film underwent a partial desorption process at 450 K. In addition the noise level in the diffraction data increased due to thiol contamination in the vacuum chamber caused by this desorption from the sample and the crystal holder at the annealing temperature which produces condensation of thiols also on the cold detector. When 450 K annealing curve is examined it can also be seen that there is a change in the slope at 350 K. This change is most probably associated with the solid–liquid phase transition which took place at 380 K during the 400 K annealing. After the 400 K pre-annealing step, the solid–liquid phase transition temperature shifts to lower values and the transition extends over a larger temperature range. Finally during annealing of HT ML to 600 K (blue trace in Fig. 4) desorption starts at 470 K and continues up to about 550 K.

Thermal and structural properties of HOD SAMs deduced from the results shown in Figs. 4 and 5 are summarized in Tables 1 and 2 along with the properties of pure MUD and ODT SAMs that were reported before [17,27]. The desorption energies reported in Table 2 were determined by performing a Redhead analysis after correcting the annealing curves shown in Fig. 4 for Debye–Waller effect and detector sensitivity.

In Fig. 6 diffraction patterns and thermal behavior of HOD, MUD and ODT SAMs are shown for comparison. Diffraction data summarized in Figs. 5 and 6 indicate that at 300 K and higher surface temperatures (during growth or annealing) HOD SAMs adopt a unit cell structure identical to that of MUD SAMs. However due to large size of the HOD molecules the resulting films were more disordered then pure MUD or ODT SAMs and helium scattering signal measured on HOD SAMs were very poor and the noise level was high. In previous helium diffraction measurements, too, the film order for chains longer than 10 carbons was observed to deteriorate with increasing chain length due to the increasing flexibility of the thiol molecules with increasing chain length [17,28]. The LT ML diffraction pattern, on the other hand, was much poorer and extracting a crystal structure from the diffraction data was not possible.

The desorption behavior of the HOD seems to be a combination of MUD and ODT and a single but broad SR intensity rise can be seen (Figs. 4 and 6) which is due to desorption from two different states with close desorption energies. This behavior is similar to what was observed for MUD previously and the corresponding desorption energies are 138 kJ/mol and 146 kJ/mol, respectively.

Table 1
Unit cell parameters for the striped phases of MUD, ODT, and HOD SAMs.

Molecule	Length[a] (Å)	p	Lattice constant (Å)	Lattice constant/2 (Å)	Difference[b] (Å)
MUD[c]	15.8	×11.8[d]	34.0 (0.184 Å^{-1})	17.0	1.2
ODT[c]	23.6	×18	51.9 (0.121 Å^{-1})	26.0	2.4
HOD	41.1	×11.8	34.0 (0.184 Å^{-1})		

[a] Reported values are the theoretical distances, calculated at AM1 level, from the center of sulfur atom to the center of furthest hydrogen atom in thiols and from the center of H atom at one end to the center of the H atom at the other end in the disulfides.
[b] Difference of the length of the molecule and the value of lattice constant/2.
[c] Reported values for MUD and ODT are taken from Ref. [17].
[d] In Ref. [26] p was reported to be 12.

Table 2
Melting temperature and the desorption energies for the striped phases of MUD, ODT, and HOD SAMs.

Molecule	Melting temperature[a] (K)	Desorption energy (kJ/mol)		
		ML		
		Desorption 1 (kJ/mol)	Desorption 2 (kJ/mol)	Desorption 3 (kJ/mol)
MUD[b]	400	118	136, 141	150
ODT[b]	400	135	154	
HOD	380	138	146	

[a] Since the melting transitions are not sharp (see Figs. 3 and 5) here approximate temperatures where melting starts are given.
[b] Reported values for MUD and ODT are taken from Ref. [17].

4. Conclusion

HOD SAMs grown in vacuum by means of supersonic molecular beam deposition (SMBD) were studied by helium diffraction. Two different lying down monolayer phases were identified. The low temperature (LT) was observed to form only when the film was grown at low substrate temperatures ($T \approx 200$ K) and irreversibly transformed into a different phase after annealing to 300 K. This high temperature (HT) phase could also be formed directly by depositing the HOD SAM at 300 K or higher substrate temperature. While the crystal structure of the LT phase could not be determined due to poor diffraction pattern of this phase, the diffraction pattern of the HT phase was similar to that of mercaptoundecanol (MUD) SAMs reported before in the literature. For the HT ML phase desorption from two different chemisorbed states with adsorption energies of 138 kJ/mol and 146 kJ/mol was observed.

Acknowledgment

This work was supported by the Scientific and Technological Research Council of Turkey, TÜBİTAK, Grant No. 209T084.

References

[1] F. Schreiber, Prog. Surf. Sci. 65 (2000) 151–256.
[2] J.C. Love, L.A. Estroff, J.K. Kriebel, R.G. Nuzzo, G.M. Whitesides, Chem. Rev. 105 (2005) 1103–1169.
[3] C. Vericat, M.E. Vela, G. Benitez, P. Carro, R.C. Salvarezza, Chem. Soc. Rev. 39 (2010) 1805–1834.
[4] Z. Matharu, A.J. Bandodkar, V. Gupta, B.D. Malhotra, Chem. Soc. Rev. 41 (2012) 1363–1402.
[5] N.J. Tao, Nat. Nanotechnol. 1 (2006) 173–181.
[6] E. Albayrak, S. Duman, G. Bracco, M.F. Danisman, Appl. Surf. Sci. 268 (2013) 98–102.
[7] M. Jaschke, H. Schonherr, H. Wolf, H.J. Butt, E. Bamberg, M.K. Besocke, H. Ringsdorf, J. Phys. Chem. 100 (1996) 2290–2301.
[8] G. Nelles, H. Schonherr, M. Jaschke, H. Wolf, M. Schaub, J. Kuther, W. Tremel, E. Bamberg, H. Ringsdorf, H.J. Butt, Langmuir 14 (1998) 808–815.
[9] M.W. Tsao, J.F. Rabolt, H. Schonherr, D.G. Castner, Langmuir 16 (2000) 1734–1743.
[10] J. Noh, M. Hara, Langmuir 16 (2000) 2045–2048.
[11] S.M. Flores, A. Shaporenko, C. Vavilala, H.J. Butt, M. Schmittel, M. Zharnikov, R. Berger, Surf. Sci. 600 (2006) 2847–2856.
[12] T. Takami, E. Delamarche, B. Michel, C. Gerber, H. Wolf, H. Ringsdorf, Langmuir 11 (1995) 3876–3881.
[13] S.F. Chen, L.Y. Li, C.L. Boozer, S.Y. Jiang, J. Phys. Chem. B 105 (2001) 2975–2980.
[14] T. Ishida, W. Mizutani, N. Choi, H. Ogiso, H. Azehara, H. Hokari, U. Akiba, M. Fujihira, I. Kojima, H. Tokumoto, Colloids Surf., A: Physicochem. Eng. Aspects 154 (1999) 219–225.
[15] T. Ishida, S. Yamamoto, W. Mizutani, M. Motomatsu, H. Tokumoto, H. Hokari, H. Azehara, M. Fujihira, Langmuir 13 (1997) 3261–3265.
[16] K. Heister, D.L. Allara, K. Bahnck, S. Frey, M. Zharnikov, M. Grunze, Langmuir 15 (1999) 5440–5443.
[17] E. Albayrak, M.F. Danisman, J. Phys. Chem. C 117 (2013) 9801–9811.
[18] M.F. Danisman, B. Ozkan, Rev. Sci. Instrum. 82 (2011).
[19] E. Albayrak, M.F. Danisman, Appl. Surf. Sci. 295 (2014) 54–58.
[20] D. Miller, in: G. Scoles (Ed.), Atomic and Molecular Beam Methods, Oxford University Press, New York, NY, 1992, p. 14.
[21] M.F. Danisman, L. Casalis, G. Bracco, G. Scoles, J. Phys. Chem. B 106 (2002) 11771–11777.
[22] P.A. Redhead, J.P. Hobson, Vacuum 15 (1965), 25-&.
[23] M.G. Roper, R.G. Jones, Phys. Chem. Chem. Phys. 10 (2008) 1336–1346.
[24] R. Rousseau, V. De Renzi, R. Mazzarello, D. Marchetto, R. Biagi, S. Scandolo, U. del Pennino, J. Phys. Chem. B 110 (2006) 10862–10872.
[25] G.E. Poirier, W.P. Fitts, J.M. White, Langmuir 17 (2001) 1176–1183.
[26] G.H. Yang, G.Y. Liu, J. Phys. Chem. B 107 (2003) 8746–8759.
[27] Y.C. Yang, T.Y. Chang, Y.L. Lee, J. Phys. Chem. C 111 (2007) 4014–4020.
[28] N. Camillone, C.E.D. Chidsey, G.Y. Liu, T.M. Putvinski, G. Scoles, J. Chem. Phys. 94 (1991) 8493–8502.